J Mater Sci (2011) 46:123–130
DOI 10.1007/s10853-010-4862-0

Wear behavior of an aluminum alloy processed by equal-channel angular pressing

Chuan Ting Wang · Nong Gao · Robert J. K. Wood · Terence G. Langdon

Received: 30 June 2010 / Accepted: 21 August 2010 / Published online: 8 September 2010

Abstract Wear tests were conducted on an aluminum Al-1050 alloy after processing by equal-channel angular pressing (ECAP). The results show that the coefficient of friction remains unchanged after processing by ECAP, but there is a decrease in the wear resistance and a mass loss that increases with increasing numbers of ECAP passes. The results are consistent with a wear mechanism map and confirm the occurrence of a severe wear mechanism. The decreasing wear resistance after ECAP is attributed to the significant grain refinement introduced by ECAP and the lack of a strain hardening capability.

Introduction

Processing through the application of severe plastic deformation (SPD) has become important over the last decade for the production of metals having ultrafine grain sizes [1]. Several SPD techniques are now available and the most promising are equal-channel angular pressing (ECAP) [2], high-pressure torsion (HPT) [3], and accumulative roll bonding (ARB) [4, 5]. In general, the ultrafine-grained materials produced using these techniques exhibit superior mechanical properties including high strength [6], enhanced fatigue properties [7] and, if the grains are reasonably stable at elevated temperatures, excellent superplastic forming capabilities [8].

Most of the studies conducted to date have focused on the microstructural evolution during SPD processing [9, 10] or the subsequent mechanical properties of the metals attained using these processes [11, 12]. However, the novel and often extraordinary properties offered by SPD processing means that these materials have potential uses in many applications ranging from precision instruments [13] to MEMS devices [14, 15] and biomedical and dental implants [16, 17].

In order to make better use of materials processed by SPD, it is very important to study their wear resistance. In practice, the wear of a component leads to an increased clearance and to a loss of precision in moving structural parts and, conversely, a high wear resistance may yield a longer service life. Nevertheless, despite the clear importance of wear in industrial applications, there are only a limited number of reports to date describing the wear characteristics of metals processed by SPD. Table 1 summarizes the information currently available for a range of ultrafine-grained materials processed by ECAP, ARB, surface mechanical attrition treatment (SMAT) and hydrostatic extrusion (HE) [18–33]. It is apparent from inspection of Table 1 that there is no consistent effect of SPD processing on the wear properties of materials since in some experiments SPD leads to an increase in the wear resistance, in others there is no significant effect and in others the wear resistance decreases. In practice, it is important to note that the wear property is a system property that is influenced, or even significantly affected, by a range of factors including the load level, the sliding

C. T. Wang · R. J. K. Wood
National Centre for Advanced Tribology at Southampton, School of Engineering Sciences, University of Southampton, Southampton SO17 1BJ, UK

C. T. Wang · N. Gao · T. G. Langdon
Materials Research Group, School of Engineering Sciences, University of Southampton, Southampton SO17 1BJ, UK

T. G. Langdon (✉)
Departments of Aerospace and Mechanical Engineering and Materials Science, University of Southern California, Los Angeles, CA 90089-1453, USA
e-mail: langdon@usc.edu

Table 1 Wear properties of materials processed by SPD

Material	SPD method	Wear rig	Lubrication condition	Effect of SPD on friction coefficient	Effect of SPD on wear resistance	Reference
Al–Al_3Ti	ECAP	Block-on-disk	N/A	N/A	No effect	Sato et al. [18]
Al–2,3,5%Cu	ECAP	Pin-on-disk	Unlubricated	N/A	Increases	Abd El Aal et al. [19]
Al–12% Si	ECAP	Pin-on-disk	Unlubricated	N/A	Decreases	Kucukomeroglu [20]
Al-1100	ARB	Pin-on-disk	Unlubricated	N/A	Decreases	Kim et al. [21]
Al-5052	ARB	Pin-on-disk	Unlubricated	N/A	Decreases	Kim et al. [21]
Al-6061	ARB	Pin-on-disk	Unlubricated	N/A	Decreases	Kim et al. [22]
Cu–10%Al–4%Fe	ECAP	Ring-on-block	Unlubricated	Reduced	Increases	Gao and Cheng [23–25]
Mg AZ61 alloy	ECAP	Pin-on-disk	Unlubricated	N/A	No effect	Kim et al. [22]
Sn–11.5%Sb–5.5%Cu	ECAP	Pin-on-disk	Lubricated	Reduced	Increases	Korshunov et al. [26]
			Unlubricated	N/A	Decreases	
Low carbon steel	SMAT	Reciprocating sliding tester	Unlubricated	Reduced	Increases	Wang et al. [27]
Low carbon steel	ECAP	Pin-on-disk	Unlubricated	N/A	Decreases	Kim et al. [21]
Ti	ECAP		Unlubricated	Reduced	Increases	Stolyarov et al. [28]
Ti	ECAP	SRV oscillating tester	Unlubricated	No effect	Increases	La et al. [29]
Ti	HE	Pin-on-disk	Unlubricated	N/A	No effect	Garbacz et al. [30]
			Various conditions	N/A	Decreases	Garbacz et al. [30]
Ti	ECAP	Pin-on-disk	Unlubricated	N/A	No effect	Purcek et al. [31]
TiNi	ECAP	Ring-on-block	Unlubricated	N/A	Increases	Cheng et al. [32]
Zn–40%Al–2% Cu–2%Si	ECAP	Pin-on-disk	Unlubricated	Reduced	Increases	Purcek et al. [33]

velocity, the use of any lubricants, and the properties of the counter surface. The variability in results documented in Table 1 demonstrates that more information is needed, and especially systematic experiments are required, in order to reach definitive conclusions concerning the effect of SPD processing on the wear properties of different materials.

The present investigation was initiated to study the wear behavior of an Al-1050 alloy after processing by ECAP. This alloy was selected because it is single phase, it has a simple f.c.c. crystal structure, and extensive information is already available on the properties of aluminum-based alloys after processing by ECAP. The wear properties were investigated using a reciprocating dry sliding wear tester with the testing conducted without any lubrication. Following testing, the debris and worn surfaces were examined using various analytical procedures.

Experimental material and procedures

The investigation used a commercial Al-1050 aluminum alloy having a composition close to Al–0.25% Fe–0.15% Si (in wt%). The alloy was supplied as rods with diameters of 9.5 mm and these rods were cut into individual billets having lengths of ~65 mm. The billets were processed by ECAP at room temperature for 1, 2, 4, and 8 passes, respectively, using a pressing speed of 0.5 mm s^{-1} and an ECAP die having an angle of 90° between the two channels and an outer arc of curvature of 20° at the point of intersection of the two channels. The principles of processing by ECAP were described in an earlier report [34] and it can be shown that these two angles lead to an imposed strain of ~1 on each passage through the die [35]. The billets were pressed using processing route Bc in which each billet is rotated in the same sense by 90° around the longitudinal axis between each pass through the die [36], where route Bc was selected because it leads most expeditiously to a reasonably homogeneous array of ultrafine grains separated by a high fraction of high-angle boundaries [37].

Dry sliding wear tests were conducted on both the as-received alloy and the alloy after processing by ECAP using a Phoenix TE77 high-frequency reciprocating test rig as illustrated schematically in Fig. 1. These tests were performed at a temperature of 20 ± 2 °C and under a relative humidity of 55 ± 5%. The samples for the wear tests were machined into plates having dimensions of 45 × 8 × 2.5 mm^3 and each plate was mechanically ground to 4000-grit SiC paper and then washed in acetone in an ultrasonic bath for 15 min. In this condition prior to testing, the average surface roughness was about 0.7 μm.

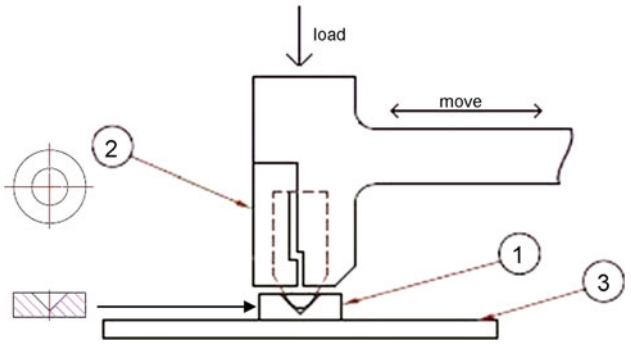

Fig. 1 Schematic illustration of the high-frequency reciprocating test rig used for the wear tests: *1* counter surface, *2* holder, *3* sample fixed in position

The counter surface used in these tests had a diameter of 12 mm which gave a contact area between the two surfaces of about 90 mm^2 and the counter pin was made of phosphor bronze with a hardness of 200 Hv. The edge of the counter surface was rounded and the counter surface pin was pressed and driven by an indenter during sliding. This design was used in order to inhibit edge cutting. Two loads of 5 and 23 N were used in this study and the apparent contact stresses were estimated as 5.6×10^{-2} and 2.6×10^{-1} MPa, respectively. During testing, the stroke length of the oscillating motion was $\sim$8.9 mm and the reciprocating frequency was 1 Hz which gave an average sliding velocity of the order of 17.9 ± 0.1 mm s^{-1}.

Before and after the wear tests, the Vickers microhardness was measured using a Matsuzawa Seiki MHT-1 microhardness tester with a load of 100 g and using a dwell time of 15 s. The mass loss of each sample in the wear test was measured using a Mettler AE240 microbalance having an accuracy of 0.1 mg. Grain sizes were recorded after ECAP using electron back-scatter diffraction (EBSD). The microstructures of the worn surfaces were analyzed using scanning electron microscopy with energy dispersion spectroscopy (SEM–EDS) using a JEOL JSM 6500 instrument and energy dispersive X-ray spectrometry was conducted with an INCA EDX analyser. The topology of the surface roughness and three-dimensional surface profiles were recorded using a XYRIS 2000 TL/CL metrology system produced by TAICAAN.

Experimental results

Microstructure and hardness after processing

In the as-received condition, the grain size of the alloy was $\sim$44 μm. Measurements by EBSD after ECAP gave average grain sizes of $\sim$15, $\sim$11, $\sim$4.9, and $\sim$1.3 μm after 1, 2, 4, and 8 passes, respectively, where the grain size

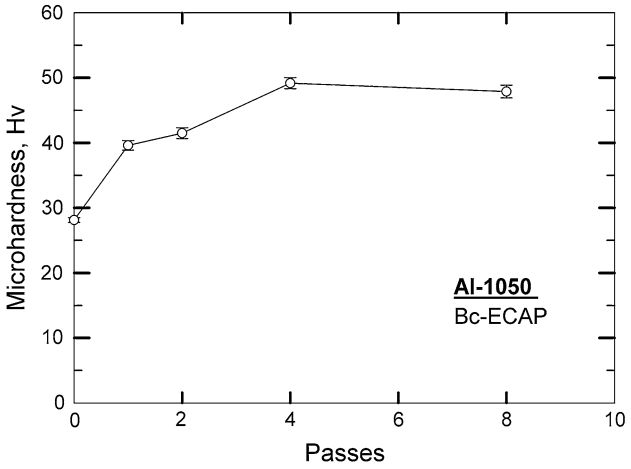

Fig. 2 Microhardness versus number of passes after processing by ECAP

after 8 passes is similar to grain sizes reported in earlier investigations using high-purity [9, 10, 38, 39] and commercial purity [40] aluminum. Figure 2 shows the variation of the microhardness with the number of passes of ECAP before the wear tests. As anticipated from earlier studies [6, 41], the hardness increases significantly after processing by ECAP.

Wear behavior of the as-received and ECAP processed samples using a dry sliding test

The average values of the coefficients of friction during sliding testing are shown in Fig. 3, for both the 5 and 23 N testing conditions. For these experiments, the sampling rate of the friction transducer was 1 Hz and the test continued for 1500 s so that each point corresponds to an average value from 1,500 datum points. It is readily apparent from Fig. 3 that ECAP has essentially no influence on the

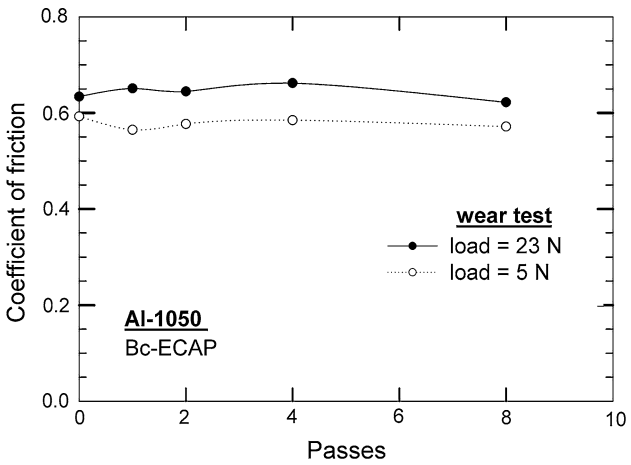

Fig. 3 Coefficient of friction versus number of passes for the two loading conditions

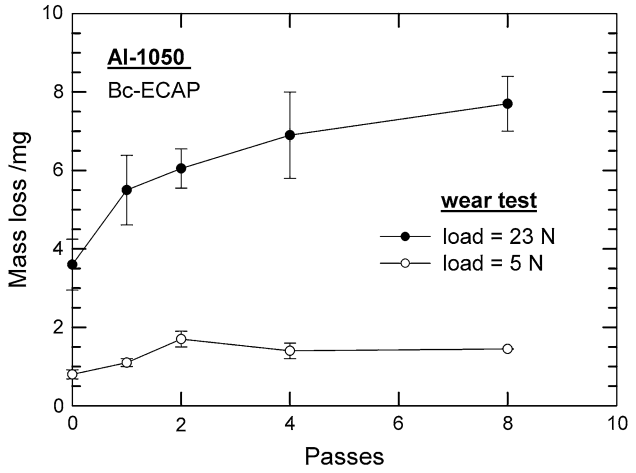

Fig. 4 Mass loss versus number of passes for the two loading conditions

measured coefficients of friction under the two loading conditions used in this study. Thus, under a load of 23 N the coefficients of friction varied from 0.62 to 0.66 whereas under a load of 5 N the coefficients of friction were slightly lower at 0.56–0.59.

The mass loss of the samples after the wear test is shown in Fig. 4, for the two different loading conditions. It has been shown theoretically that the mass loss may be estimated using the Archard equation [42] given by

$$V = K\frac{SL}{3H} \tag{1}$$

where V is the volume worn away during testing, S is the total sliding distance, L is the normal load, H is the hardness of the softer surface, and K is a dimensionless wear coefficient specific to the sample under test. Since the samples processed by ECAP have a higher hardness than the as-received sample, as shown in Fig. 2, it is reasonable to anticipate from Eq. 1 that they will experience a smaller mass loss. Nevertheless, it is evident from Fig. 4 that the samples processed by ECAP exhibit a larger mass loss and, in addition, this mass loss increases with increasing numbers of passes for the samples tested under a load of 23 N. Because of the apparent differences between the samples tested with loads of 23 and 5 N, these samples are examined separately in the following two sections.

Testing under a load of 23 N for 1500 s

All samples tested under a load of 23 N for 1500 s exhibited exceptionally severe wear with evidence for much white debris that became detached from the samples. An SEM study showed that the morphologies of the worn surfaces of all samples were reasonably similar and examples are shown in Fig. 5 for (a) the as-received condition and after ECAP through (b) 1 pass and (c) 8 passes.

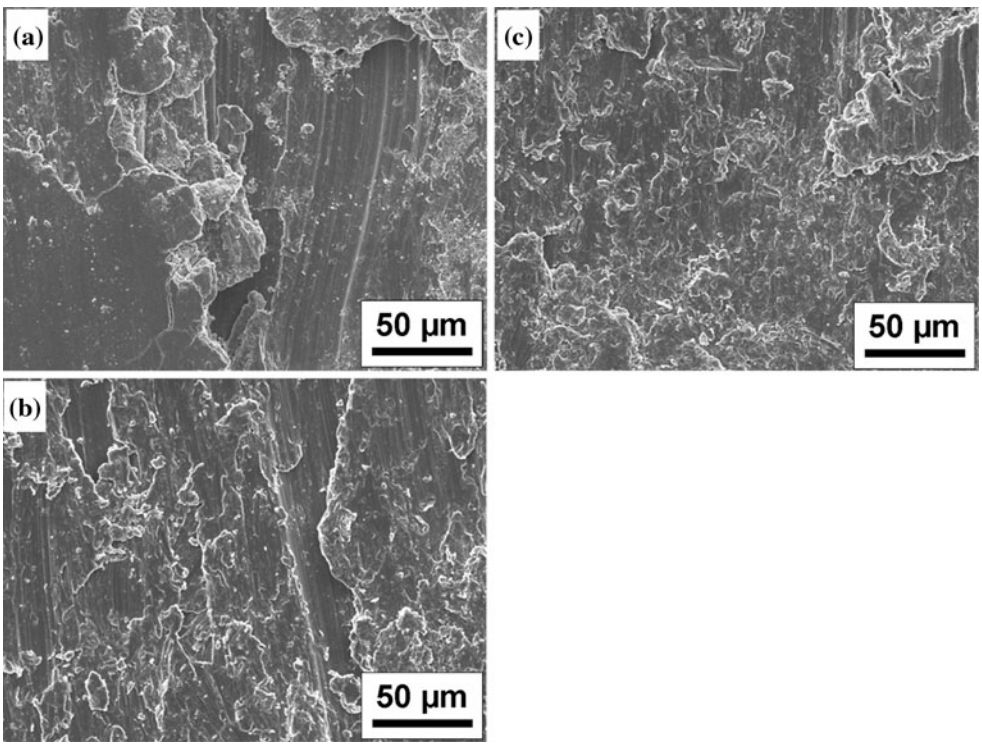

Fig. 5 SEM micrographs of worn surfaces after wear tests under a load of 23 N: **a** as-received material, **b** after 1 pass of ECAP, and **c** after 8 passes of ECAP

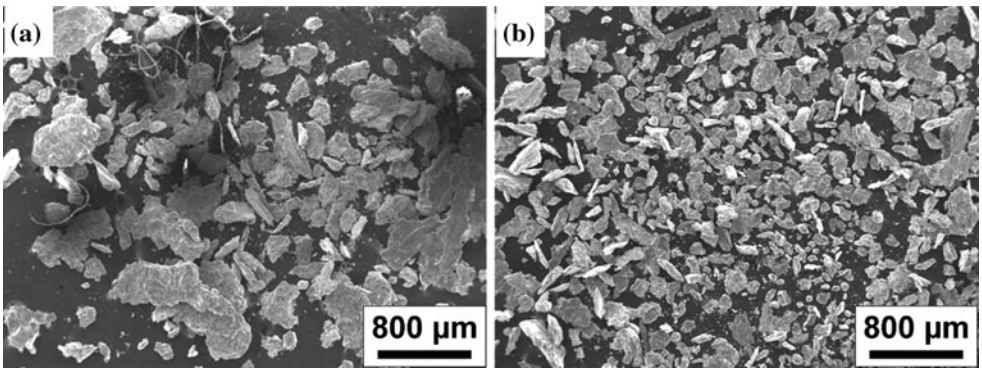

Fig. 6 Wear debris of samples under a sliding load of 23 N: **a** for the as-received condition and **b** after 8 passes of ECAP

The appearance of the worn surfaces of the samples is typical of adhesive wear and this has been widely reported for soft and ductile materials such as copper, aluminum, and gold [43, 44]. Figure 6 shows the wear debris for (a) the as-received condition and (b) after ECAP through 8 passes. Some of the debris in Fig. 6 has a higher appearance probably because of charging effects associated with the orientations of the debris on the SEM holder. It is readily apparent from Fig. 6 that the size of the debris is significantly smaller after processing by ECAP.

Testing under a load of 5 N for 1500 s

During the sliding wear test under the lower load of 5 N, it was observed that the wear debris was a mixture of white flake-like particles and black powder. This is shown in Fig. 7 where (a) and (b) are low and high magnification images, respectively: the lower portions of Fig. 7 show the EDS analyses of the small areas marked with rectangles in the upper images. It was noted that the white flake-like particles visible in Fig. 7a were observed from the beginning of each wear test whereas the black powder in Fig. 7b became visible at some point during the test. Similar results were also reported in an earlier investigation [45] and it was proposed, in agreement with the current EDS analyses, that the white particles are monolithic aluminum detached from the sample.

Material transfer was also evident with aluminum transferred onto the pin surface. Figure 8 shows the counter surface and appropriate EDS analyses after 8 passes of ECAP: the image on the left is at a low magnification and the small area within the rectangle is given at a higher magnification on the right. These observations show that the counter surface is partially covered by transferred fragments and the EDS analyses confirm these transferred fragments are mixed components of aluminum and aluminum oxide. Many of the earlier studies used steel as the counter surface [45–48] and mechanically mixed layers (MML) were widely observed on the surfaces of aluminum samples when using an Al-steel wearing system. In the

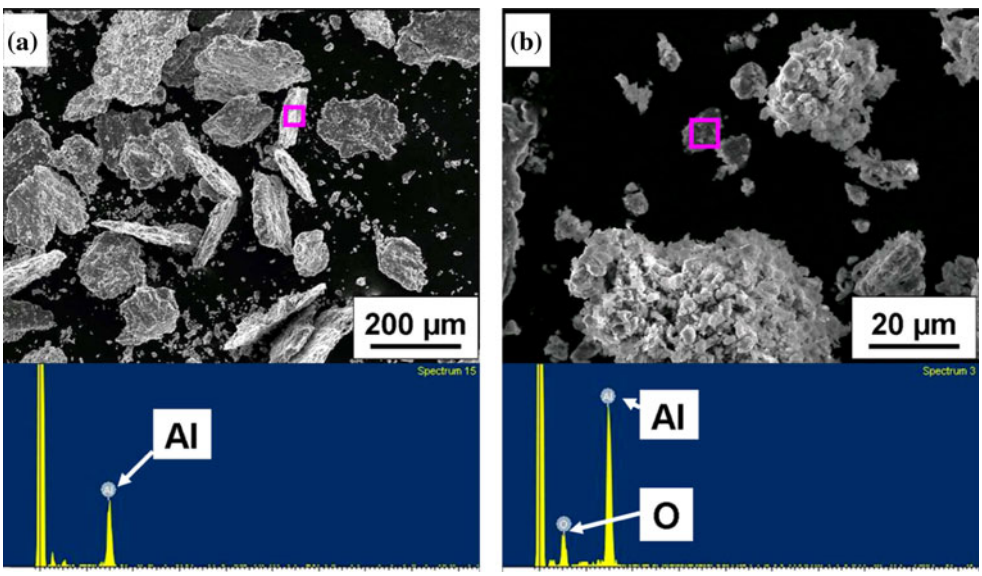

Fig. 7 EDS analysis of wear debris from 8 passes of ECAP after wear test using a load of 5 N for **a** low and **b** high magnifications

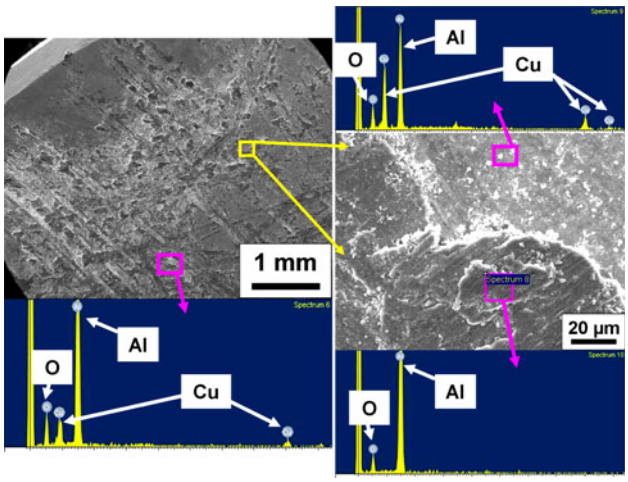

Fig. 8 EDS analysis of the counter surface against 8 passes of ECAP sample after wear test using a load of 5 N

present investigation, the use of a phosphor bronze as the counter surface led to material transfer but not to the formation of MML.

Evidence for surface deformation was also visible on the worn surfaces of the samples after wear testing. Figure 9 shows an example using a load of 5 N after 8 passes of ECAP where the topological three-dimensional profile is shown at upper left, a portion of the worn surface is shown at lower right and two EDS analyses are included for the small rectangles marked in the image. The three-dimensional profile shows that the worn surface is made up of low-lying areas and some higher flats. It was found by EDS analysis that these low-lying areas were close to pure aluminum and the higher flats contained a high fraction of oxygen. It is evident from the color-coding in Fig. 9 that the separation distance between the high flats and the low-lying areas is typically of the order of several tens of microns, where this is similar to the thickness of the flake debris in Fig. 7. This suggests that during the wear test the flakes are detached from the sample and leave pits which join at a later stage to from low-lying areas.

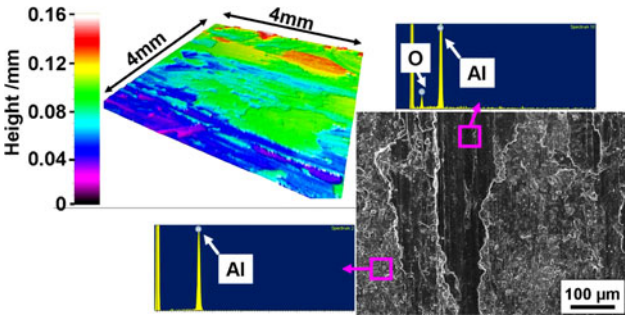

Fig. 9 Three-dimensional analysis and EDS analysis of the worn surface of an 8 pass ECAP sample after wear test using a load of 5 N

Discussion

The results of this investigation provide useful information on the wear characteristics of an Al-1050 alloy processed by ECAP to produce exceptional grain refinement. Processing by ECAP increases the hardness of the material, it leads to little or no change in the coefficients of friction when wear testing under two different loading conditions of 5 and 23 N, there is a transfer of material to the counter surface during testing and there is also a very significant mass loss when using the higher load of 23 N. Studies of the debris, worn surfaces, and wear rates all indicate that these two loading conditions produce a severe wear mechanism. However, the higher hardness introduced by ECAP leads to a higher mass loss than in the as-received material and this appears to be inconsistent with the conventional Archard relationship given in Eq. 1.

The development of wear mechanism maps was the first attempt to delineate the wear processes in a simple pictorial form [49] and to provide information that may be correlated with observed transitions between different wear processes [50]. The maps were developed using the following relationships for the normalized pressure at the sliding interface, $\bar{F}$, and the normalized velocity, $\bar{v}$, where the latter corresponds to the sliding velocity in wear divided by the velocity of heat flow [49]:

$$\bar{F} = \frac{F}{A_n H_o} \tag{2}$$

and

$$\bar{v} = \frac{v r_o}{a} \tag{3}$$

where F is the normal force (N), A_n is the nominal contact area (m^2); H_o is the room temperature hardness ($N\ m^{-2}$), v is the sliding speed ($m\ s^{-1}$), r_o is the radius of the nominal contact area, and a is the thermal diffusivity. Subsequently, this approach was used to develop a dry sliding map for aluminum and its alloys [51] and the result is shown in Fig. 10 where the normalized pressure is plotted logarithmically against the normalized velocity. The dashed lines delineate transitions between the different wear mechanisms and each separate wear mechanism is dominant within the designated area.

Calculations suggest the orders of magnitude values in the present investigation are $\bar{F} \approx 10^{-4}$ since there is little difference in the hardness values for the different samples and $\bar{v} \approx 10$. Therefore, inserting these values into the wear mechanism map in Fig. 10 leads to the lower oval designated contact (A), which suggests the occurrence of an oxidation-dominated wear for the two loading conditions used in this study. However, this is not consistent with the

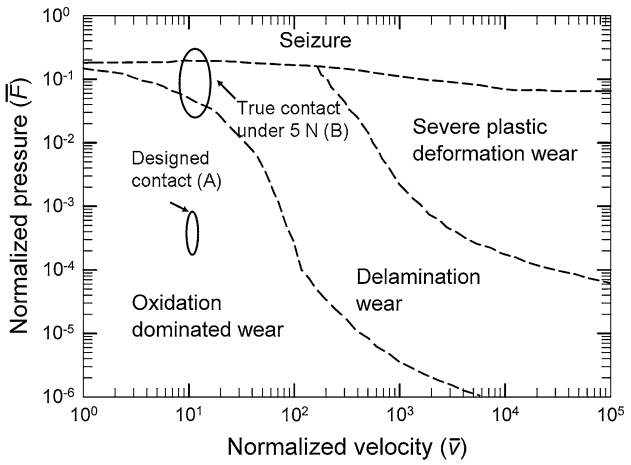

Fig. 10 A wear mechanism map for aluminum and its alloys [51] showing the apparent designated area for the current wear tests at *A* and the corrected area at *B* when incorporating additional information concerning the wear process

flake-like debris shown in Figs 6 and 7 and the clear evidence for a severe wear mechanism.

The dimensional wear coefficient, k, is widely used to compare wear rates in different classes of materials and it is defined by

$$k = \frac{V}{SL} \tag{4}$$

Calculation suggests that under the load of 23 N the dimensional wear coefficient for the sample processed by ECAP through 4 passes is $\sim 4.1 \times 10^{-6}$ mm^2 N^{-1} while under the load of 5 N the dimensional wear coefficient for a similar sample is $\sim 3.8 \times 10^{-6}$ mm^2 N^{-1}. That means that wear under the two conditions is dominated by a severe wear mechanism with a wear rate higher than 10^{-8} mm^2 N^{-1} [52].

In practice, the wear mechanism was significantly more severe than expected and this appears to be due to two reasons. First, the hardness of the pin material was higher in these tests than the disk material and this wear system often results in a more severe wear mode [53]. Second, during the initial time of sliding the true contact area is initially smaller than the apparent contact area due to the nature of the two surfaces [54]. Under these conditions for a load of 5 N, the contact stress of the connecting areas is higher than initially expected and this suggests the true contact stress is probably close to the upper oval in Fig. 10. For these testing conditions, it is therefore reasonable to anticipate a transition towards a severe wear mechanism. Thus, during this initial period the surface of the softer material becomes significantly deformed and this generates extensive debris by adhesion such that the mass loss measured in Fig. 4 is experienced primarily in this initial period.

As the test continues, black particles are produced containing high fractions of oxygen, where these particles are spread over the sliding surface and lead to a decrease in the wear rate [44, 45, 52]. There is some uncertainty regarding the formation process for these fine black particles but they may be produced by a complex mechanical alloying process [52] or through a hydroxide or similar high-oxygen content phase [55]. As the total test duration was not long, the size and the amount of this black debris were not comparable to the plate-like debris and accordingly the total mass loss was due primarily to the loss of the plate-like debris.

Finally, it is necessary to address the apparent disagreement with the Archard relationship given in Eq. 1 since processing by ECAP leads to a higher hardness but also, as shown in Fig. 4 for the samples tested under a load of 23 N, to an increase in the mass loss with increasing numbers of passes in ECAP. This decrease in the wear resistance after processing by ECAP is consistent with very recent results for the Al-1100 and Al-5052 alloys processed by ARB [21], where the lower wear resistance was attributed to the lack of significant strain hardening in the alloys subjected to SPD processing. This conclusion is in agreement with the present results and it is further supported by a recent experimental observation, also for an aluminum alloy, that the strain hardening capability of the alloy is essentially exhausted after two passes of ECAP [56]. The apparent discrepancy may be explained in part by the nature of the microstructure introduced by the ECAP process since processing by ECAP leads not only to a refined grain size but also to the introduction of high energy non-equilibrium grain boundaries [57, 58] and to an increase in both the average grain boundary misorientation angle and the total fraction of high-angle boundaries with increasing numbers of ECAP passes [10]. These microstructural changes are not incorporated in Eq. 1 but they appear to account for the increased mass loss after larger numbers of ECAP passes.

Summary and conclusions

1. An Al-1050 alloy was processed by ECAP leading to a refined microstructure and increased hardness. Samples processed by ECAP were subjected to wear testing under loads of 5 and 23 N.
2. The samples processed by ECAP have similar coefficients of friction to the unprocessed alloy at least for the two loading conditions used in this investigation but the ECAP processing leads to a decrease in the wear resistance and to a mass loss that increases with increasing numbers of ECAP passes.
3. The wear results show good agreement with a wear mechanism map when it is recognized that the true

contact stress of the connecting areas is significantly higher than expected. The map predicts a transition towards the occurrence of a severe wear mechanism.

4. The results suggest the wear tests under both loads are dominated by a severe wear mechanism and the decreasing wear resistance after ECAP is due to the characteristics of grain refinement in the ECAP procedure and the inherent loss of a strain hardening capability.

Acknowledgements This work was supported by a studentship from the School of Engineering Sciences at the University of Southampton together with a scholarship from the China Scholarship Council (CTW). Partial support was provided by EPSRC under Grant No EP/D00313X/1 and by the National Science Foundation of the United States under Grant No. DMR-0855009.

References

1. Valiev RZ, Estrin Y, Horita Z, Langdon TG, Zehetbauer MJ, Zhu YT (2006) JOM 58(4):33
2. Valiev RZ, Langdon TG (2006) Prog Mater Sci 51:881
3. Zhilyaev AP, Langdon TG (2008) Prog Mater Sci 53:893
4. Saito Y, Tsuji N, Utsunomiya H, Sakai T, Hong RG (1998) Scripta Mater 39:1221
5. Tsuji N, Saito Y, Utsunomiya H, Tanigawa S (1999) Scripta Mater 40:795
6. Horita Z, Fujinami T, Nemoto M, Langdon TG (2000) Metall Mater Trans 31A:691
7. Höppel HW, Kautz M, Xu C, Murashkin M, Langdon TG, Valiev RZ, Mughrabi H (2006) Int J Fatigue 28:1001
8. Horita Z, Furukawa M, Nemoto M, Barnes AJ, Langdon TG (2000) Acta Mater 48:3633
9. Iwahashi Y, Horita Z, Nemoto M, Langdon TG (1998) Acta Mater 46:3317
10. Kawasaki M, Horita Z, Langdon TG (2009) Mater Sci Eng A524:143
11. Valiev RZ, Krasilnikov NA, Tsenev NK (1991) Mater Sci Eng A137:35
12. Valiev RZ, Alexandrov IV, Zhu YT, Lowe TC (2002) J Mater Res 17:5
13. Kim WJ, Sa YK (2006) Scripta Mater 54:1391
14. Estrin Y, Janecek M, Raab GI, Valiev RZ, Zi A (2007) Metall Mater Trans 38A:1906
15. Qiao XG, Gao N, Moktadir Z, Kraft M, Starink MJ (2010) J Micromech Microeng 20:045029
16. Latysh V, Krallics G, Alexandrov I, Fodor A (2006) Curr Appl Phys 6:262
17. Valiev RZ, Semenova IP, Latysh VV, Rack H, Lowe TC, Petruzelka J, Dluhos L, Hrusak D, Sochova J (2008) Adv Eng Mater 10:B15
18. Sato H, Elhadad S, Sitdikov O, Watanabe Y (2008) Mater Sci Forum 584–586:971
19. Abd El Aal MI, El Mahallawy N, Shehata FA, Abd El Hameed M, Yoon EY, Kim HS (2010) Mater Sci Eng A527:3726
20. Kucukomeroglu T (2010) Mater Des 31:782
21. Kim YS, Yu HS, Shin DH (2009) Int J Mater Res 100:871
22. Kim YS, Ha JS, Kim WJ (2004) Mater Sci Forum 449–452:597
23. Gao LL, Cheng XH (2007) Tribol Lett 27:221
24. Gao LL, Cheng XH (2008) Wear 265:986
25. Gao LL, Cheng XH (2008) Mater Sci Eng A473:259
26. Korshunov LG, Noskova NI, Korznikov AV, Chernenko NL, Vil'danova NF (2009) Phys Met Metallogr 108:519
27. Wang ZB, Tao NR, Li S, Wang W, Liu G, Lu J, Lu K (2003) Mater Sci Eng A352:144
28. Stolyarov VV, Shuster LS, Migranov MS, Valiev RZ, Zhu YT (2004) Mater Sci Eng A371:313
29. La P, Ma J, Zhu YT, Yang J, Liu W, Xue Q, Valiev RZ (2005) Acta Mater 53:5167
30. Garbacz H, Gradzka-Dahlke M, Kurzydlowski KJ (2007) Wear 263:572
31. Purcek G, Saray O, Kul O, Karaman I, Yapici GG, Haouaoui M, Maier HJ (2009) Mater Sci Eng A517:97
32. Cheng X, Li Z, Xiang G (2007) Mater Des 28:2218
33. Purcek G, Saray O, Kucukomeroglu T, Haouaoui M, Karaman I (2010) Mater Sci Eng A527:3480
34. Furukawa M, Horita Z, Nemoto M, Langdon TG (2001) J Mater Sci 36:2835. doi:10.1023/A:1017932417043
35. Iwahashi Y, Wang J, Horita Z, Nemoto M, Langdon TG (1996) Scripta Mater 35:143
36. Furukawa M, Iwahashi Y, Horita Z, Nemoto M, Langdon TG (1998) Mater Sci Eng A257:328
37. Oh-ishi K, Horita Z, Furukawa M, Nemoto M, Langdon TG (1998) Metall Mater Trans 29A:2011
38. Nakashima K, Horita Z, Nemoto M, Langdon TG (1998) Acta Mater 46:1589
39. Terhune SD, Swisher DL, Oh-ishi K, Horita Z, Langdon TG, McNelley TR (2002) Metall Mater Trans 33A:2173
40. Salem AA, Langdon TG, McNelley TR, Kalidindi SR, Semiatin SL (2006) Metall Mater Trans 37A:2879
41. Horita Z, Fujinami T, Nemoto M, Langdon TG (2001) J Mater Process Technol 117:288
42. Archard JF (1953) J Appl Phys 24:981
43. Kuo SM, Rigney DA (1992) Mater Sci Eng A157:131
44. Rigney DA (2000) Wear 245:1
45. Zhang J, Alpas AT (1997) Acta Mater 45:513
46. Pramila BN, Biswas SK (1991) Acta Metall Mater 39:833
47. Li XY, Tandon KN (2000) Wear 245:148
48. Tandon KN, Li XY (1997) Scripta Mater 38:7
49. Lim SC, Ashby MF (1987) Acta Metall 35:1
50. Lim SC, Ashby MF, Brunton JH (1987) Acta Metall 35:1343
51. Liu Y, Asthana R, Rohatgi P (1991) J Mater Sci 26:99. doi:10.1007/BF00576038
52. Hiratsuka K, Muramoto K (2005) Wear 259:467
53. Rigney DA (1994) Wear 175:63
54. Blau PJ (1981) Wear 71:29
55. Kim HJ, Karthikeyan S, Rigney D (2007) Wear 263:849
56. Cetlin PR, Aguilar MTP, Figueiredo RB, Langdon TG (2010) J Mater Sci 45:4561. doi:10.1007/s10853-010-4384-9
57. Wang J, Horita Z, Furukawa M, Nemoto M, Tsenev NK, Valiev RZ, Ma Y, Langdon TG (1993) J Mater Res 8:2810
58. Horita Z, Smith DJ, Nemoto M, Valiev RZ, Langdon TG (1998) J Mater Res 13:446